Appl. Phys. B 64, 25–36 (1997)

Applied Physics B Lasers and Optics

Simulation of laser dynamics and active Q-switching in Tm,Ho:YAG and Tm:YAG lasers

J. M. Sousa, J. R Salcedo, V. V. Kuzmin

INESC - Centro de Optoelectrónica, R. José Falcão, 110, 4000 Porto-Portugal
(Fax: + 351-2/2008487, E-mail: jsousa@yang.inescn.pt)

Received: 7 March 1996/Accepted: 28 May 1996

Abstract. We developed a detailed rate equation model to study laser dynamics and active Q-switching in Tm,Ho:YAG and Tm:YAG lasers. The simulation results agreed well with published experimental data, as well as provided new insights for optimizing pulse generation.

Recently, Tm,Ho:YAG and Tm:YAG lasers have become important as sources of long laser pulses (in the μs range), appropriate for coherent laser radar applications and atmospheric probing, as well as for medical applications [1]. Laser radar applications, by Doppler signal processing arguments, impose this fairly long pulse duration: a 1 μs pulse allows wind velocity discrimination up to 1 ms^{-1}, as required by the avionics industry for laser radars to be of significant potential and interest [2].

Both laser systems oscillate in the 2 μm eye safe wavelength region; in addition, both have broad ($\approx$ 4 nm) absorption lines centered at about 780 nm, a wavelength region where efficient pumping diodes are available.

From the laser side, however, the generation of only one smooth pulse of near microsecond duration will normally require some type of appropriately designed active Q-switch. The careful study of laser dynamics becomes relevant for these applications, because Tm,Ho:YAG lasers, in particular, readily generate multiple pulses.

Both Tm,Ho:YAG and Tm:YAG have long upper-laser-level lifetimes, in the range 5.5–10 ms [3–5], and small laser-transition effective cross-sections (7×10^{-21} cm^2 at 2.097 μm [3] and 1.5×10^{-21} cm^2 at 2.01 μm [6] respectively), making them suitable candidates to generate high-power, single-frequency, 100 ns to 1 μs laser pulses.

Tm,Ho:YAG suffers from several drawbacks. Under typical experimental conditions, only about 50% of the stored energy in Tm transfers from Tm to Ho; in addition, Q-switching tends to generate multiple pulses instead of just one smooth pulse, due to the limited energy extraction from the laser media [7–9].

The lack of availability of a detailed dynamical model of these lasers provided us with the basic motivation to develop such a model.

The model includes explicitly the fine structure of all energy levels involved, as well as the effect of ground-state depletion of both Tm and Ho populations.

The model is based on detailed rate equations, and it includes no adjustable parameters for simulating laser dynamics, Q-switching included. The model generates all outputs in real physical units, as μs, W and J, and takes into account the processes of pumping, energy transfer from Tm to Ho (in the case of a Tm,Ho:YAG crystal), laser-level manifolds and energy splittings, ground-state depletion, and various other effects described below, all important to study the laser dynamics and Q-switched pulse-generation processes in these lasers.

We may also use our model to optimize other laser parameters such as cavity geometry's, doping levels and active modulator regimes. As a result, we are now able to perform quite precise simulations of laser dynamics and pulse generation in three-level solid-state lasers. It would also be easy to adapt the model to study other types of solid-state lasers like waveguide and fiber lasers.

The present work will concentrate on the laser dynamics aspects, and will ignore other complementary considerations like specific pumping geometry's, cavity designs, thermal effects as well; we do not take into account the effect of pump and laser-mode cross-sectional spatial distribution, as well as the longitudinal inhomogeneity in both pumping and inversion spatial distributions. For this specific purpose, a full three-dimensional rate equation extension is needed.

As previously mentioned, the model explicitly includes depletion of the ground-state populations, for both Tm and Ho. This aspect is important, since achieving a population inversion requires an excited-state population of the order of the corresponding doping concentration. As a direct consequence, ground-state depletion must be taken into account if we want our model to generate

meaningful results, since varying ground-state populations will affect

a) The process of absorption of the pumping energy.
b) The energy distribution between Tm^{3+} and Ho^{3+} ions.
c) The process of light amplification itself.

A detailed one-dimensional rate equation approach provides the basis for our model. This approach is valid only for laser dynamics slow enough when compared to the laser resonator round-trip time, and this is certainly appropriate in our studies. We also suppose that the Tm and Ho upper and lower manifolds are in thermal equilibrium.

Furthermore, we included an analytical calculation of the lasing threshold and optimal crystal length for CW operation for both Tm:YAG and Tm,Ho:YAG lasers, taking into account three-dimensional Gaussian pumping and laser-mode distributions.

1 Theory

1.1 Energy-level diagrams for Tm,Ho:YAG and Tm:YAG

Figure 1 shows the appropriate energy-level diagrams for Tm:YAG and Tm,Ho:YAG.

There seems to be an unresolved inconsistency in the literature regarding the upper-laser-level nomenclature of Tm. In our model, we assume the upper-laser level of Tm as $^3F_4$ [7, 8, 10, 11] and not $^3H_4$, as sometimes reported [3, 12–14].

In the model, we consider continuous pumping near 780 nm. Fast decay from $^3H_4$ populates the metastable level $^3F_4$. For large enough Tm doping concentration, the cross relaxation process may lead to a total quantum efficiency for $^3F_4$ close to 2 [3, 15, 16]. In this work, we consider the lasing action to occur in Tm only (Tm:YAG laser) and Ho only (Tm,Ho:YAG laser), as shown in Fig. 1.

We performed an extensive literature search to compile all reported energies for the energy-level fine structure [10–13, 17–19]. Table 1 summarizes the result of this compilation.

Our model assumes as parameters what seem to be the best estimates for the energy levels, taken from published, reliable, experimental data, or from published theoretical estimates if such data are not available [10, 17]. In all cases, we took a "best-estimate" approach. We should note, however, that the temperature dependence of these sublevel energies is not known to date.

Many possible laser transitions may occur between the upper- and lower-laser-level manifolds, due to the level fine structure. We chose specific laser transitions after a careful study of this aspect, corresponding to specific sublevels. Our model assumes the following specific laser levels throughout:

Tm:YAG $14 \rightarrow 8$ (energy 5556 $cm^{-1} \rightarrow 610\ cm^{-1}$)
$\lambda = 2.022\ \mu m$

Tm,Ho:YAG $19 \rightarrow 12$ (energy 5232 $cm^{-1} \rightarrow 457\ cm^{-1}$)
$\lambda = 2.094\ \mu m$

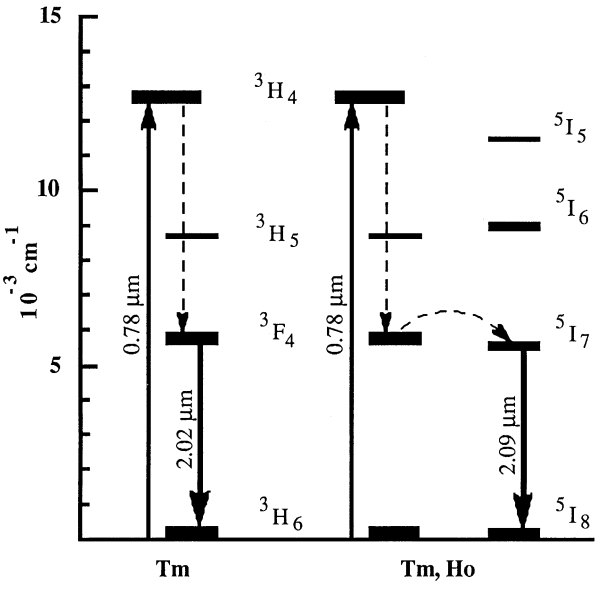

Fig. 1. Energy-level diagrams for Tm:YAG and Tm,Ho:YAG

This specific choice agrees with the laser frequencies as measured experimentally [14], and comes very close to the most detailed theoretical estimates available [11, 19]. In any case, we may note that small alterations in the specific sublevels involved will not change the model results appreciably.

In our model, we consider that, in equilibrium, the population distribution among the various fine structure sublevels follows the Boltzmann distribution; hence, the population fractions $f^0_{Tm,Ho}$ and $f^1_{Tm,Ho}$ for the manifolds belonging to the lower- and upper-laser levels of Tm^{3+} and Ho^{3+}, are

$$f^{0.1}_{Tm,Ho} = \frac{e^{(-E^{0,1}/kT)}}{\sum_m e^{(-E_m/kT)}}. \tag{1}$$

In this expression, the sum over m is the sum over the appropriate manifold, k is the Boltzmann constant, T is the temperature and $E^{0,1}$ refers to the particular energy of the lower-laser level, E^0, and of the upper-laser level, E^1, that we consider in the model, as previously described, each one of them within the corresponding manifold. More specifically, for Tm, E^0 is the energy associated with sublevel $\{8\}$ in the lower-level manifold, and E^1 is the energy associated with sublevel $\{14\}$ in the upper-level manifold. A similar argument applies for Ho. Table 1 shows the known published results for the energy splittings, and indicates our specific choices for this study; it also shows the calculation results for $f^0_{Tm}, f^1_{Tm}, f^0_{Ho}, f^1_{Ho}$, in the temperature range of $+20$ to $-40°C$, for transitions $\{19\} \rightarrow \{12\}$ in Ho and $\{14\} \rightarrow \{18\}$ in Tm.

1.2 Energy transfer mechanisms in Tm,Ho:YAG

For Tm,Ho:YAG, we chose a simple phenomenological energy-transfer mechanism for inclusion in the model. We describe the $Tm \Leftrightarrow Ho$ energy transfer process by the

Table 1. Compilation of published results for energy splittings of Ho:YAG and Tm:YAG. Table shows our choices for sublevel energies, as well as calculations of f^0 and f^1 for various temperatures

Ho:YAG
518 (Lower manifold)

Sublevel >		1	2	3	4	5	6	7	8	9	10	11	12	13	14	15	16	17	f_0 (293 K)	Δ	f_0(233 K)	Δ
Ref.	Type																					
[17]	Experiment	0	4	41	51	138	145	151	160		418	448	457	498	506	520	531		0.0168	1.4%	0.0108	1.6%
[17]	Calculation	2	5	39	42	137	147	151	159	399	419	447	456	503	510	513	534	536	0.0168	0.9%	0.0107	1.0%
[18]	Experiment	0		42	54	141			161		418	448	464	494		519		535	0.0169	1.8%	0.0108	2.2%
[20]	Calculation	0	2	40	44	142	147	152	154	395	418	452	458	492	501	503	520	522	0.0167	0.5%	0.0107	0.6%
[20]	Calculation	0	3	32	44	116	119	120	129	393	411	432	467	480	496	499	505	506	0.0158	− 4.6%	0.0100	− 5.4%
Our choice		0	4	41	51	138	145	151	160	399	418	448	457	498	506	520	531	536	0.0168	1.4%	0.0108	1.6%

517 (Upper manifold)

Sublevel >		18	19	20	21	22	23	24	25	26	27	28	29	30	31	32	f_1 (293 K)	Δ	f_1(233 K)	Δ
Ref.	Type																			
[17]	Experiment	5229	5232	5243	5250	5303	5312	5320	5341	5352	5375	5395	5404	5418	5455		0.1112	0.3%	0.1219	5.1%
[17]	Calculation	5228	5231	5242	5252	5304	5313	5322	5339	5355	5379	5393	5400	5415	5488	5490	0.1125	1.4%	0.1143	− 1.4%
[18]	Experiment	5228	5230	5244	5251	5304	5312	5318	5338	5350	5371	5377	5406	5416	5455		0.1119	0.9%	0.1139	− 1.8%
[20]	Calculation	5227	5230	5238	5248	5302	5313	5320	5338	5351	5379	5394	5399	5415	5481	5483	0.1118	0.8%	0.1136	− 2.0%
[20]	Calculation	5224	5228	5237	5246	5268	5287	5289	5326	5350	5371	5375	5384	5397	5479	5481	0.1070	− 3.5%	0.1161	0.1%
Our choice		5229	5232	5243	5250	5303	5312	5320	5341	5352	5375	5395	5404	5418	5455	5490	0.1112	0.3%	0.1219	5.1%

Tm:YAG
3H6 (Lower manifold)

Sublevel >		1	2	3	4	5	6	7	8	9	10	11	12	13	f_0 (293 K)	Δ	f_0(233 K)	Δ
Ref.	Type																	
[10]	Experiment	0	27	216	241	247	252	588	610		690		730		0.0148	0.2%	0.0080	0.8%
[10]	Calculation	− 3	24	215	225	262	253	518	610	650	684	698	751	765	0.0146	− 1.4%	0.0079	− 1.0%
[13]	Experiment	0	27	215	241	245	448	547	588	610					0.0172	16.7%	0.0096	20.8%
[12]	Calculation	0	27	218	228	256	266	520	613	652	687	701	754	767	0.0146	− 1.4%	0.0079	− 1.0%
[12]	Calculation	0	13	278	285	295	354	600	660	701	708	731	740	762	0.0127	− 14.1%	0.0064	− 19.5%
Our choice		0	27	216	241	247	252	588	610	650	690	698	730	765	0.0148	0.2%	0.0080	0.8%

3F4 (Upper manifold)

Sublevel >		14	15	16	17	18	19	20	21	22	f_1 (293 K)	Δ	f_1(233 K)	Δ
Ref.	Type													
[10]	Experiment	5556	5736	5832	5901	6041	6108	6170	6224	6233	0.4681	− 2.4%	0.5660	− 2.6%
[10]	Calculation	5536	5757	5810	5912	6040	6111	6164	6228	6243	0.4975	3.8%	0.6030	3.7%
[13]	Experiment	5557	5737	5809	5875	5907	6046	6148	6177		0.4307	− 10.2%	0.5242	− 9.8%
[12]	Calculation	5539	5760	5813	5915	6043	6114	6166	6231	6246	0.4975	3.8%	0.6030	3.7%
[12]	Calculation	5571	5796	5864	5933	6076	6149	6241	6243	6261	0.5031	4.9%	0.6104	5.0%
Our choice		5556	5736	5832	5901	6041	6108	6170	6224	6233	0.4681	− 2.4%	0.5660	− 2.6%

following equations:

$$\frac{d[N^1_{Tm}f - N^1_{Ho}(1-f)]}{dt} = -\frac{N^1_{Tm}f - N^1_{Ho}(1-f)}{\tau_{Tm\leftrightarrow Ho}}, \quad (2)$$

$$\frac{d(N^1_{Tm} + N^1_{Ho})}{dt} = -\frac{N^1_{Tm} + N^1_{Ho}}{\tau}, \quad (3)$$

where τ is the coupled-state upper-level lifetime (phenomenological definition), $\tau_{Tm\leftrightarrow Ho}$ is the energy transfer time (phenomenological definition) f is the net energy-transfer efficiency to Ho.

For typical doping concentrations, the characteristic energy transfer time from Tm to Ho is between 5 and 20 μs, according to published data [3, 20]. We may treat the $^3F_4$ and $^5I_7$ levels as one coupled system, since this energy transfer time is much smaller than either of the $^3F_4$ and $^5I_7$ level lifetimes. So we assume the following assumptions in our model: after energy migration among the Tm^{3+} ions, a fraction of the energy will transfer to the Ho^{3+} ions because its $^5I_7$ level is quasi-resonant with the $^3F_4$ Tm level.

1.3 Ground-state depletion

In the case of continuous pumping, we may consider the $^3F_4$ (Tm) and $^5I_7$ (Ho) manifolds as being in quasi-thermal equilibrium, in agreement with published reports [21, 22], as such, the net energy transfer to Ho in equilibrium, is

$$f = \frac{N^0_{Ho}\sum_i e^{(-E_i/kT)}}{N^0_{Ho}\sum_i e^{(-E_i/kT)} + N^0_{Tm}\sum_j e^{(-E_j/kT)}}. \quad (4)$$

In this expression, N^0_{Ho} and N^0_{Tm} are the ground-state populations for Ho^{3+} and Tm^{3+}, respectively, the sums over the i and j are sums over $^5I_7$ (Ho) and $^3F_4$ (Tm) crystal-field splittings, respectively, E_i and E_j are the corresponding energy values associated with these splittings, k is the Boltzmann constant and T is the temperature.

The previous equation is equivalent to similar equations used in the literature [3], with one important difference, it used the ground-state populations (N^0_{Ho} and N^0_{Tm}) as the proper weighting factors instead of the more common total ion concentrations (N_{Ho} and N_{Tm}). This subtle but important difference allows us to consider the ground-state depletion explicitly, a feature absent from previously published models.

In reality, the net energy-transfer efficiency, f, will depend on the ground-state population N^0_{Ho} directly, and not on the total ion concentration N_{Ho}, since N_{Ho}, by itself, does not tell us the fraction of Ho ions already in the excited state. As a result, and to include ground-state depletion of the energy-transfer process explicitly, we must include the last equation as written.

To optimize the laser system, we should also consider the dependence of coupled-state upper-level lifetime τ on the pumping rate R [3, 23]. In a Tm,Ho:YAG laser, the effective upper-level lifetime decreases to 0.19 ms at a pumping intensity of about 0.5 kW cm^{-2}; in Tm:YAG it decreases to 4.3 ms at the same pumping intensity [14], to 3 ms at 2 kW cm^{-2} and to 1.8 ms at 10 kW cm^{-2} [23]. Two independent effects lead to the observed decrease in τ; ground-state depletion and up-conversion. As will be shown later, these effects affect these two types of laser differently. In Tm:YAG, ground-state depletion is the dominant effect, but in Tm,Ho:YAG up-conversion overcomes ground-state depletion as the main reason for the decrease in the value of τ.

1.4 Tm,Ho:YAG model

The appropriate rate equations for a Tm,Ho:YAG laser, are

$$\frac{dN^1_{Tm}}{dt}f - \frac{dN^1_{Ho}}{dt}(1-f) = Rf - \frac{N^1_{Tm}f - N^1_{Ho}(1-f)}{\tau_{Tm\leftrightarrow Ho}} + \frac{\sigma_{Ho}c}{V}(f^1_{Ho}N^1_{Ho} - f^0_{Ho}N^0_{Ho})(1-f)q, \quad (5)$$

$$\frac{dN^1_{Tm}}{dt} + \frac{dN^1_{Ho}}{dt} = R - \frac{N^1_{Tm} - N^1_{Ho}}{\tau} - \frac{\sigma_{Ho}c}{V}(f^1_{Ho}N^1_{Ho} - f^0_{Ho}N^0_{Ho})q, \quad (6)$$

$$\frac{dq}{dt} = \frac{\sigma_{Ho}cl}{L}(f^1_{Ho}N^1_{Ho} - f^0_{Ho}N^0_{Ho})(q+1) - \frac{\gamma cq}{2L}, \quad (7)$$

$$R = \frac{P\eta L}{h\nu_p V l}[1 - e^{(-\alpha l)}], \quad (8)$$

$$\alpha = \alpha_0 \frac{N^0_{Tm}}{N_{Tm}}, \quad (9)$$

$$N^1_{Ho} + N^0_{Ho} = N_{Ho}, \quad (10)$$

$$N^1_{Tm} + N^0_{Tm} = N_{Tm}. \quad (11)$$

In these expressions:

N^1_{Tm}, N^0_{Tm} – populations of the upper $^3F_4$ and lower $^3H_6$ Tm manifolds,
N^1_{Ho}, N^1_{Ho} – populations of the upper $^5I_7$ and lower $^5I_8$ Ho, manifolds,
N_{Ho}, N_{Tm} – total doping concentrations for Ho and Tm,
q – total number of photons in the laser cavity,
R – pumping rate including the effect of pump depletion due to ground-state depletion,
α, α_0 – saturated and unsaturated (small-signal) absorption coefficient at the pumping wavelength,
P – pumping power,
η – pumping quantum efficiency,
$h\nu_p$ – energy of the pumping photons,
$\tau_{Tm\leftrightarrow Ho}$ – characteristic time for the Tm–Ho energy transfer process,
τ – upper-level lifetime for the coupled Tm–Ho system,
σ_{Ho} – cross-section for Ho $^5I_7 \leftrightarrow {}^5I_8$ lasing transition (not effective, but real),

c – speed of light in vacuum,
V – volume of the laser mode,
l – active media length,
L – optical resonator length, defined by

$$L = L_0 + (n-1)\,l, \tag{12}$$

where

L_0 – empty cavity length,
n – laser-crystal index of refraction at the pumping wavelength
γ – total logarithmic loss for one resonator round-trip including output coupling.

The presented equations describe the pumping, energy transfer and lasing processes in three-level solid-state lasers like Tm,Ho:YAG.

Equations (5) and (6) above may also be written in a slightly different form, entirely equivalent but possibly easier to visualize:

$$\frac{\mathrm{d}N^1_{\mathrm{Tm}}}{\mathrm{d}t} = R + \frac{N^1_{\mathrm{Ho}}}{\tau_{\mathrm{HT}}} - \frac{N^1_{\mathrm{Tm}}}{\tau} - \frac{N^1_{\mathrm{Tm}}}{\tau_{\mathrm{TH}}}, \tag{13}$$

$$\frac{\mathrm{d}N^1_{\mathrm{Ho}}}{\mathrm{d}t} = \frac{N^1_{\mathrm{Tm}}}{\tau_{\mathrm{TH}}} - \frac{N^1_{\mathrm{Ho}}}{\tau} - \frac{N^1_{\mathrm{Ho}}}{\tau_{\mathrm{HT}}} - \frac{\sigma_{\mathrm{Ho}}c}{V}\left(f^1_{\mathrm{Ho}}N^1_{\mathrm{Ho}} - f^0_{\mathrm{Ho}}N^0_{\mathrm{Ho}}\right)q, \tag{14}$$

where

$$\frac{1}{\tau_{\mathrm{HT}}} = \left(\frac{1}{\tau_{\mathrm{Tm}\leftrightarrow\mathrm{Ho}}} - \frac{1}{\tau}\right)(1-f), \tag{15}$$

$$\frac{1}{\tau_{\mathrm{TH}}} = \left(\frac{1}{\tau_{\mathrm{Tm}\leftrightarrow\mathrm{Ho}}} - \frac{1}{\tau}\right)f. \tag{16}$$

This alternative form for the main rate equations may be more convenient for later incorporation of additional processes such as up-conversion. Up-conversion is not included directly in our model at this time. Recent publications [24–27] dealing with this tissue suggest that the appropriate coefficients are not yet well known; moreover, up-conversion is not the only process that may reduce the upper-level lifetime with increasing pumping intensity. In this work, we use experimental figures for the upper-level lifetime, assuming that it is relatively easy to measure the exact dependence of this lifetime with pumping intensity.

In our model the parameter f entirely describes the energy-transfer process between Tm and Ho:

$$\frac{\tau_{\mathrm{HT}}}{\tau_{\mathrm{TH}}} = \frac{f}{1-f} = \frac{N^0_{\mathrm{Ho}}\sum_i \mathrm{e}^{-E_i/kT}}{N^0_{\mathrm{Tm}}\sum_j \mathrm{e}^{-E_j/kT}}. \tag{17}$$

If one ignores this relation, the model will reduce to the more common situation of a non-Boltzmann energy distribution among Tm and Ho ion upper levels. In this case, the ratio of the two energy-transfer rates defines the energy partition between the Tm^{3+} and Ho^{3+} ions.

We should also note that there is an alternative but equivalent way to explicitly take into account the effect of ground-state depletion on the energy transfer process, by defining the depleted time constants τ_{TH} and τ_{HT} as follows:

$$\tau_{\mathrm{HT}} = \tau^0_{\mathrm{HT}}\left(\frac{N^0_{\mathrm{Ho}}}{N_{\mathrm{Ho}}}\Big/\frac{N^0_{\mathrm{Tm}}}{N_{\mathrm{Tm}}}\right), \tag{18}$$

$$\tau_{\mathrm{TH}} = \tau^0_{\mathrm{TH}}\left(\frac{N^0_{\mathrm{Tm}}}{N_{\mathrm{Tm}}}\Big/\frac{N^0_{\mathrm{Ho}}}{N_{\mathrm{Ho}}}\right), \tag{19}$$

In these expressions, τ^0_{HT} and τ^0_{TH} are the corresponding undepleted time constants, i.e. the time constants applicable when ground-state depletion is either absent or ignored.

1.5 Tm:YAG model

Following similar arguments, the rate equations for Tm:YAG are

$$\frac{\mathrm{d}N^1_{\mathrm{Tm}}}{\mathrm{d}t} = R - \frac{N^1_{\mathrm{Tm}}}{\tau_{\mathrm{Tm}}} - \frac{\sigma_{\mathrm{Tm}}c}{V}\left(f^1_{\mathrm{Tm}}N^1_{\mathrm{Tm}} - f^0_{\mathrm{Tm}}N^0_{\mathrm{Tm}}\right)q, \tag{20}$$

$$\frac{\mathrm{d}q}{\mathrm{d}t} = \frac{\sigma_{\mathrm{Tm}}cl}{L}\left(f^1_{\mathrm{Tm}}N^1_{\mathrm{Tm}} - f^0_{\mathrm{Tm}}N^0_{\mathrm{Tm}}\right)(q+1) - \frac{\gamma cq}{2L}, \tag{21}$$

$$N^1_{\mathrm{Tm}} + N^0_{\mathrm{Tm}} = N, \tag{22}$$

where:

τ_{Tm} – lifetime of the Tm^{3+} $^4F_4$ manifold,
$f^0_{\mathrm{Tm}}, f^1_{\mathrm{Tm}}$ – populations fractions of Tm^{3+} in the $^3H_6$ and $^3F_4$ manifolds, respectively, corresponding to the previously defined laser levels and given previously by (1),
σ_{Tm} – cross-section of the Tm^{3+} $^3F_4 \rightarrow {}^3H_6$ transition
R – pumping rate, given by (8), which already includes pumping depletion, as previously described.

We may derive these equations directly from the previous rate equations for Tm,Ho:YAG if we let the energy-transfer parameter f go to zero. Moreover, we now have to explicitly include laser action for the Tm^{3+} ion, which was absent in the previous case of Tm,Ho:YAG (we assumed all laser action to occur in the Ho ion).

1.6 Threshold calculations

To calculate the lasing threshold, we consider in the model the inclusion of spatial coordinates and a normalized Gaussian intensity distribution to describe both the pumping $r_{\mathrm{p}}(r,z)$ as well as the laser mode $s_0(r,z)$ in the gain medium (assumed TEM_{00}). The equations that describe this situation, are [24]:

$$r_{\mathrm{p}}(r,s) = \frac{2\alpha_0}{\pi w_{\mathrm{p}}^2(1-\mathrm{e}^{-\alpha_0 l})}\mathrm{e}^{-(\alpha_0 z + 2r^2/w_{\mathrm{p}}^2)}, \tag{23}$$

$$s_0(r,s) = \frac{2}{\pi w_0^2 l}\mathrm{e}^{-2r^2/w_0^2}, \tag{24}$$

and

$$\iiint_{V_a} r_{\mathrm{p}}(r,z)\,\mathrm{d}V = \iiint_{V} s_0(r,z)\,\mathrm{d}V = 1. \tag{25}$$

Here, w_p and w_0 are the Gaussian radii for the pump and laser cavity modes defined by the E-field amplitudes at $r = w_p$, w_0 is their e^{-1} value at $r = 0$, the integration in the first integral is taken over the gain volume, and in the second over all laser cavity volume. As before, α_0 is the unsaturated linear absorption coefficient at the pumping wavelength.

Performing an analytical calculation for the lasing threshold pumping power, we obtain the following equations [24]:

$$P_{Th} = \frac{h\nu_p \pi l(w_p^2 + w_0^2)}{2\eta(1 - e^{-\alpha_0 l})} \frac{f_{Ho}^0 N_{Ho} + \gamma/2\sigma_{Ho} l}{(f_{Ho}^0 + f_{Ho}^1)(\tau - \tau_{Tm \leftrightarrow Ho})} f \tag{26}$$

for the case of a Tm,Ho:YAG laser, and

$$P_{Th} = \frac{h\nu_p \pi l(w_p^2 + w_0^2)}{2\eta(1 - e^{-\alpha_0 l})} \frac{f_{Tm}^0 N_{Tm} + \gamma/2\sigma_{Tm} l}{(f_{Tm}^0 + f_{Tm}^1)\tau} \tag{27}$$

for the case of a Tm:YAG laser.

In these equations, $h\nu_p$ is the pumping photon energy. From the previous equations, and by differentiation with respect to l, we may calculate the crystal length that gives the lowest lasing threshold, i.e. we may optimize the crystal length with respect to lasing threshold. We obtain the same result for both types of laser (Tm:YAG and Tm,Ho:YAG), and this result is the same as for an ordinary quasi-three-level system [24].

The condition for optimal crystal length (written for Tm,Ho:YAG) is then

$$\frac{f_{Ho}^0 N_{Ho} \sigma_{Ho}}{\alpha_0} = \frac{e^{-\alpha_0 l}}{1 - e^{-\alpha_0 l}} (f_{Ho}^0 N_{Ho} \sigma_{Ho} l - \gamma/2) \tag{28}$$

We expect this result, since varying the crystal length should not affect the energy transport process or dynamics, but only the effectiveness of pumping absorption and the reabsorption losses for the laser radiation.

2 Model validation and simulation results

We solved numerically the two sets of coupled nonlinear differential equations (described on Sect. 1), one for Tm,Ho:YAG, the other for Tm:YAG, using an adaptive-step fourth-order Runge–Kutta algorithm on a Hewlett-Packard 730 workstation. We solved both systems for free running (unmodulated) and Q-switched laser operation. We assumed a step-function modulation to represent the Q-switching process, although there is no fundamental limitation in the model to cover more complex modulation schemes. Since our main interest is TEM_{00} operation, we have restricted our attention to this case.

To completely specify the dynamics of the CW-pumped repetitively Q-switched laser, we must specify suitable initial conditions, i.e. initial-level populations and photon density. To damp out any artifact dynamics, we started with reasonable estimates for the initial conditions and allowed the simulation to run over a few modulation cycles. We took conclusions from our computations by observing the fourth or fifth-generated pulse, after noting that this was enough time to stabilize the repetitive Q-switching behavior to within better than 1% (all computed pulses after the fourth or fifth were nearly identical).

To test our model, we used specific experimental measurements reported previously for Tm:YAG and Tm,Ho:YAG lasers as test data [14], against which we compared our simulation results.

2.1 Model results for the Tm,Ho:YAG and Tm:YAG Q-switched lasers. Validation

Cavity losses had to be estimated from the results reported for a Tm:YAG laser [14]. Our model was run several times for different cavity losses until we were able to predict laser-output energies in good agreement with the experimental results. The resultant internal cavity losses (excluding output coupling) were 4.75%.

For this simulation, we also used $P = 3.9$ W, $N_{Tm} = 4\%$, $l = 0.5$ cm, $L = 94$ cm, $T = -39°C$, $T_{Out} = 2.2\%$, $\tau = 10$ ms [14], beam radius $w = 167$ μm (we estimated this beam diameter from the razor-blade measurement data reported for the 10–90% points, [14]), and $\sigma_{Ho} = 7 \times 10^{-20}$ cm^2 [3].

Figure 2 shows the calculated output-pulse energy dependence on pulse spacing, for this Tm:YAG laser, showing good agreement with the reported experimental values.

Next we used our model to compute the Q-switched operation of the Tm,Ho:YAG laser without any adjustable parameters. Figure 3 shows the computed results, for $P = 4.72$ W, $N_{Tm} = 6\%$, $N_{Ho} = 1\%$, $l = 0.3$ cm, $L = 73$ cm, $T = -38°C$, $T_{Out} = 2.2\%$, $\gamma = 6.95\%$ (4.75% internal losses and 2.2% output coupling), $\tau = 190$ μs, beam radius $w = 167\sqrt{73/94} = 147$ μm and general experimental conditions reported [14].

Figure 3 depicts the computed-pulse-energy dependence on pulse spacing, for this Tm,Ho:YAG laser, and the calculated results show good agreement with the reported experimental values.

These results also show that in this particular laser, the main reason why the effective upper-level lifetime has decreased to 190 μs [14] is up-conversion.

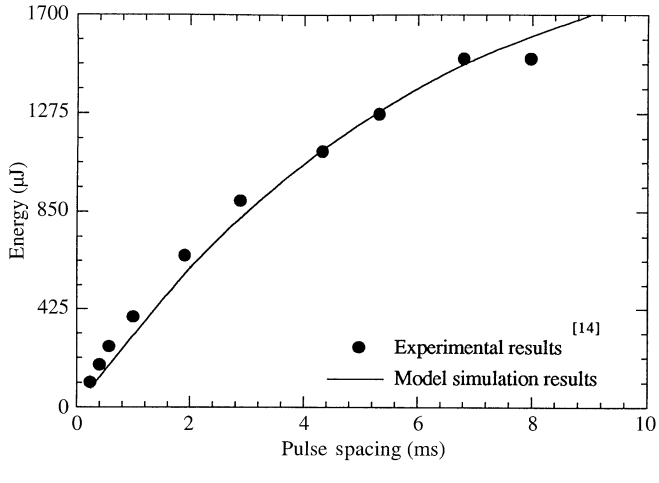

Fig. 2. Dependence of the Q-switched pulse energy on pulse temporal separation for the Tm:YAG laser

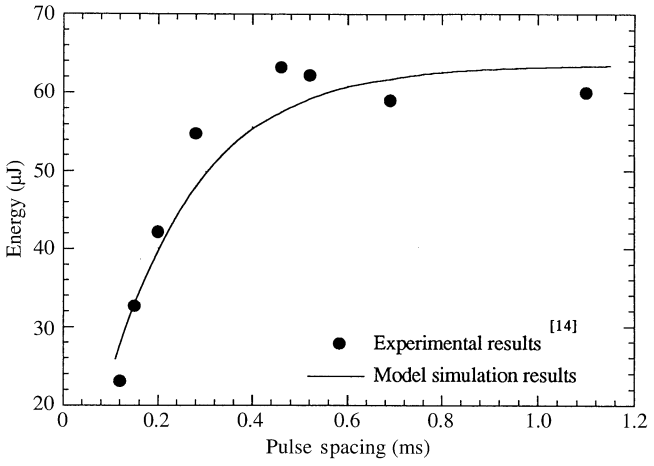

Fig. 3. Dependence of the Q-switched pulse energy on pulse temporal separation for the Tm,Ho:YAG laser

Figure 4 shows the Q-switched Tm,Ho:YAG simulation results for a 1 ms pulse separation. The computed-pulse energy is 63.2 μJ and the computed-FWHM pulsewidth is 330 ns (to be compared with the reported experimental values [14] of 60 μJ and 860 ns).

In the following section we use our computational model to investigate and compare Tm,Ho:YAG and Tm:YAG laser operation in both Q-switched and free running regimes, thus allowing a direct comparison between these two types of lasers.

For the situation of a free running regime, we investigated the dynamical processes that occur after pumping is switched on; for the situation of a Q-switched regime, we concentrated on the spiking behavior that occurs in Tm,Ho:YAG, as well as the effectiveness of the energy extraction from the Tm–Ho coupled system.

2.2 Comparison between Tm,Ho:YAG and Tm:YAG lasers

While keeping the laser parameters constant (for cavity length, mode diameter, output coupler transmission, crystal temperature, and so on), we allow the crystal length and the Ho concentration to vary and use our computational model to optimize the output-pulse energy of this laser in Q-switching regime.

We obtained an optimal crystal length $l = 0.45$ cm, and optimum Holmium concentration $N_{\mathrm{Ho}} = 0.7\%$, allowing the generation of Q-switched pulses of 70.3 μJ output energy for a pumping power of 4.72 W and pulse separation of 1 ms. This means that the optimization of the Ho concentration and crystal length allows in increase of 11% in the output energy for the specific combination of input parameters as obtained in real experiments ($l = 0.3$ cm, $N_{\mathrm{Ho}} = 1\%$). This suggests that the experimental conditions chosen [14] were actually very close from ideal; however, it should be noted that up-conversion effects would imply a reduction in N_{Ho} to maintain optimum conditions. In our computations, we kept the Tm concentration constant, since varying it would lead to

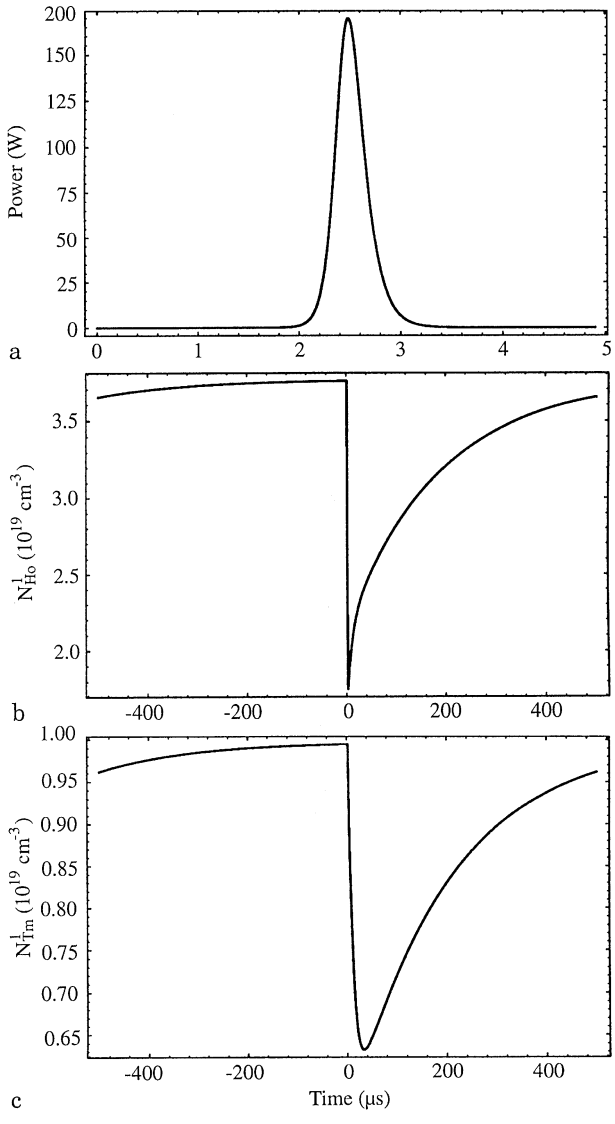

Fig. 4a–c. Computed-laser dynamics for a Q-switched Tm,Ho:YAG laser. Time origin taken as the Q-switch opening moment. **a** Output pulse, for 4.72 W pumping power and 1 kHz pulse repetition frequency. Pulse energy is 63.2 μJ and pulse duration is 330 ns, showing good agreement with experimental values [14]. **b** Excited-state Ho population dynamics. **c** Excited-state Tm population dynamics

an unpredictable change in pumping quantum efficiency and characteristic time associated with the Tm–Ho energy transfer.

We should make some additional comments: If we use (28) to optimize the crystal length, we would get a value of 0.31 cm for a 0.7% Ho concentration; however, our computational results indicate an optimum crystal length of 0.45 cm, suggesting that the optimal length (the crystal length that gives minimum lasing threshold) for CW operation does not coincide with the crystal length which maximizes the energy of the Q-switched pulses.

To ensure consistency, we performed all Tm:YAG laser calculations (doping level 4%) using the same parameters as for Tm,Ho:YAG. From (28), we calculated the optimum crystal length for CW operation to be 0.63 cm.

We also optimized the crystal length regarding maximum Q-switched output-pulse energy using our rate equation model. The result was 2.0 cm, predicting the generation of Q-switched pulses with an output energy of 2.7 mJ at a MF (modulation frequency) of 130 Hz. This is 35% larger than the 2.0 mJ calculated for a 0.63 cm crystal.

These results may be better understood by analyzing Figs. 5 and 6. Figure 5 shows the computed Tm:YAG output pulse energy dependence on crystal length, under the same experimental conditions as the Tm,Ho:YAG laser. Similarly, Fig. 6 shows the corresponding dependence for the Tm,Ho:YAG laser ($N_{Tm} = 6\%$, $N_{Ho} = 1\%$). In both figures, we mark with an arrow the optimum crystal length for CW lasing (minimizing lasing threshold). It may be observed that the optimum crystal length for Q-switching operation is larger than the optimum crystal length for CW operation.

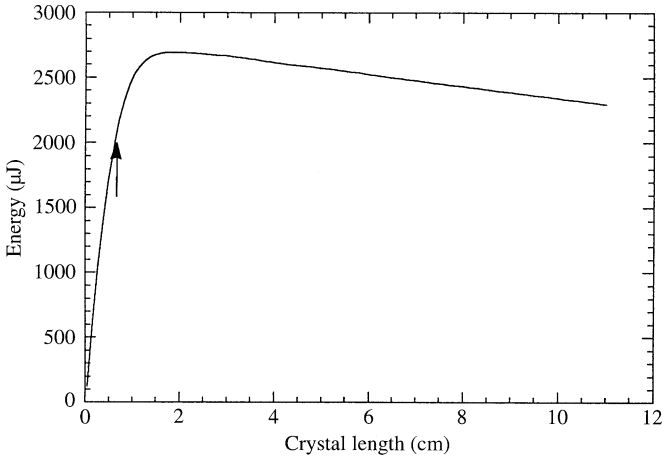

Fig. 5. Tm:YAG output pulse energy dependence on crystal length. Arrow indicates the optimum crystal length for cw operation ($N_{Tm} = 4\%$)

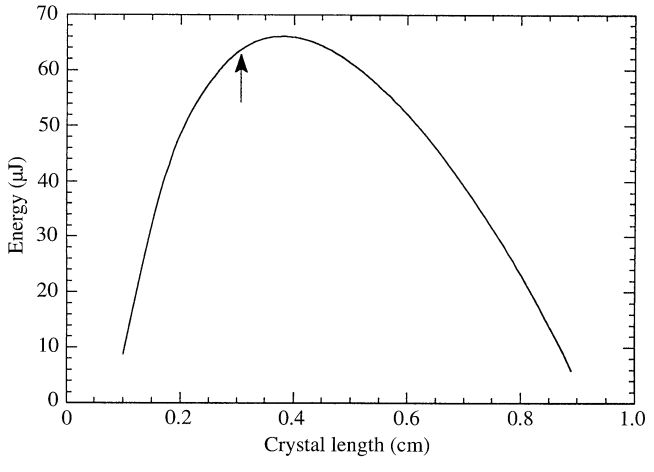

Fig. 6. Tm,Ho:YAG output pulse energy dependence on crystal length for concentrations $N_{Tm} = 6\%$, $N_{Ho} = 1\%$. Arrow indicates the optimum length for cw operation

To compare Tm:YAG and Tm,Ho:YAG lasers, we used the model to compute the laser-output pulse energy for a Tm:YAG laser ($N_{Tm} = 4\%$, $l = 2.0$ cm, other parameters the same as for Tm,Ho:YAG) for a MF of 1 kHz. The result was 573 μJ, and this is about an order of magnitude higher than the value 70.3 μJ predicted for the Tm,Ho:YAG laser. Even for this MF, about ideal for a Tm:YAG laser and certainly far from ideal for a Tm:YAG laser (assuming an upper-level lifetime 10 ms), a Tm:YAG laser is able to generate much more powerful Q-switched pulses. This coincides with known published experimental results, although it is not obvious if one considers that the CW output powers of these lasers are approximately equal.

2.3 Laser dynamics in Tm,Ho:YAG lasers

To investigate the spiking behavior experimentally observed for this type of lasers, we considered a loss modulation function with a longer duration of low loss period (300 μs), larger than the 50 μs used in our previous calculations. This open time allows the observation of several spikes and their detailed study using the computer model.

We made computations for $l = 0.45$ cm, $N_{Ho} = 0.7\%$, a pumping power of 4.72 W and a pulse separation of 1 ms. Figure 7a and b shows the results for the calculated laser output. Under these conditions, 73% of the total stored energy was transferred to the Ho^{3+} ions, and 45% of this transferred energy was extracted in the first pulse, This suggests that a significant amount of remaining energy (about 67% of the total stored energy) will be available to support additional pulses.

Our calculations indicate that the first pulse has an energy of 69.3 μJ and a FWHM pulsewidth of 0.3 μs; and the second pulse, appearing 50 μs afterwards, has an energy of 12.2 μJ and a FWHM pulsewidth of 1.81 μs. The second and the following pulses do not resemble normal Q-switched pulses, but resemble relaxation oscillation pulses instead. To allow a direct comparison, Fig. 7c shows the calculation results for the same laser in a normal mode regime, assuming as initial conditions $N^1_{Tm} = N^1_{Ho} = 0$.

For a better understanding of the spiking process, we repeated the calculations for different modulation frequencies. With increasing Q-switching repetition rate (MF), the effectiveness of the energy extraction from the active media decreases, and the time delay between the Q-switched pulse and the first spike afterwards decreases; with increasing repetition rate, also, the amplitude of the Q-switched pulses decreases and their duration increases, whereas the remaining spiking pulses remain approximately unchanged (Fig. 8). We observed that when the MF increases up to 8 kHz, the first pulse does not resemble a Q-switched pulse at all, but resembles a normal mode spiking pulse instead. Decreasing the pumping power will lead to similar results as increasing the MF.

To investigate the effect of the slow and incomplete energy transfer from Tm to Ho, we repeated the calculations for the same parameters except the Tm–Ho energy transfer time was now allowed to assume the extreme

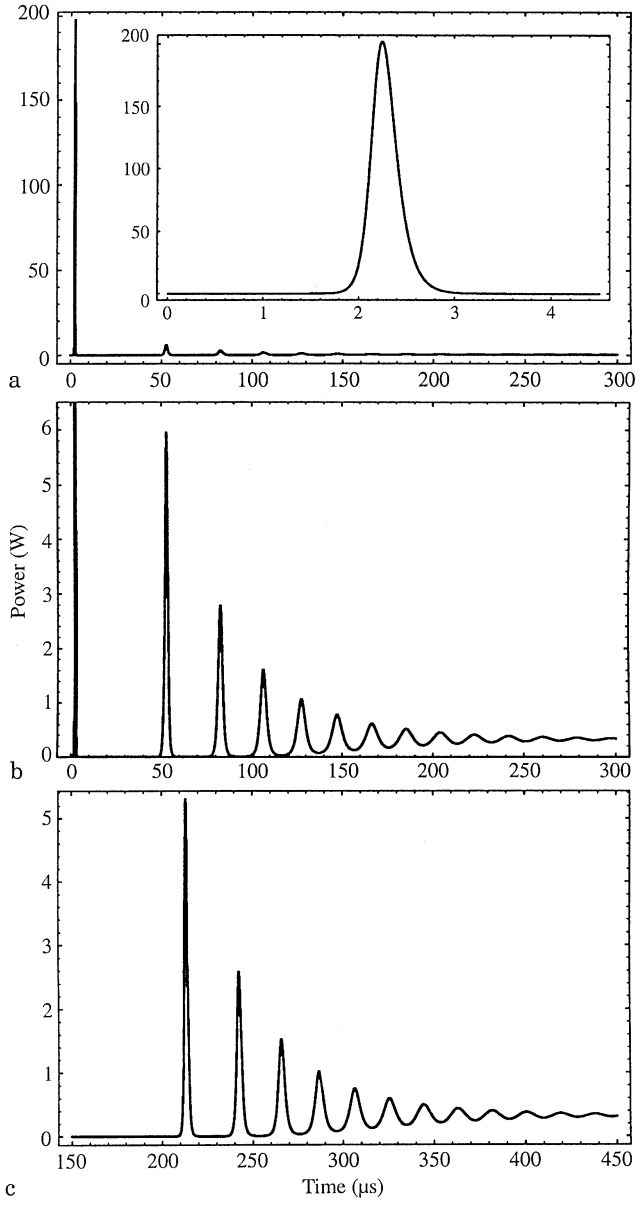

Fig. 7a–c. Computed output pulses of Tm,Ho:YAG laser (assuming $\tau_{Tm\leftrightarrow Ho} = 10$ μs). **a** Laser in Q-switching regime. Inset shows Q-switched pulse. **b** Expanded vertical scale view. **c** Laser in normal-mode regime. Similarity to (b) is evident

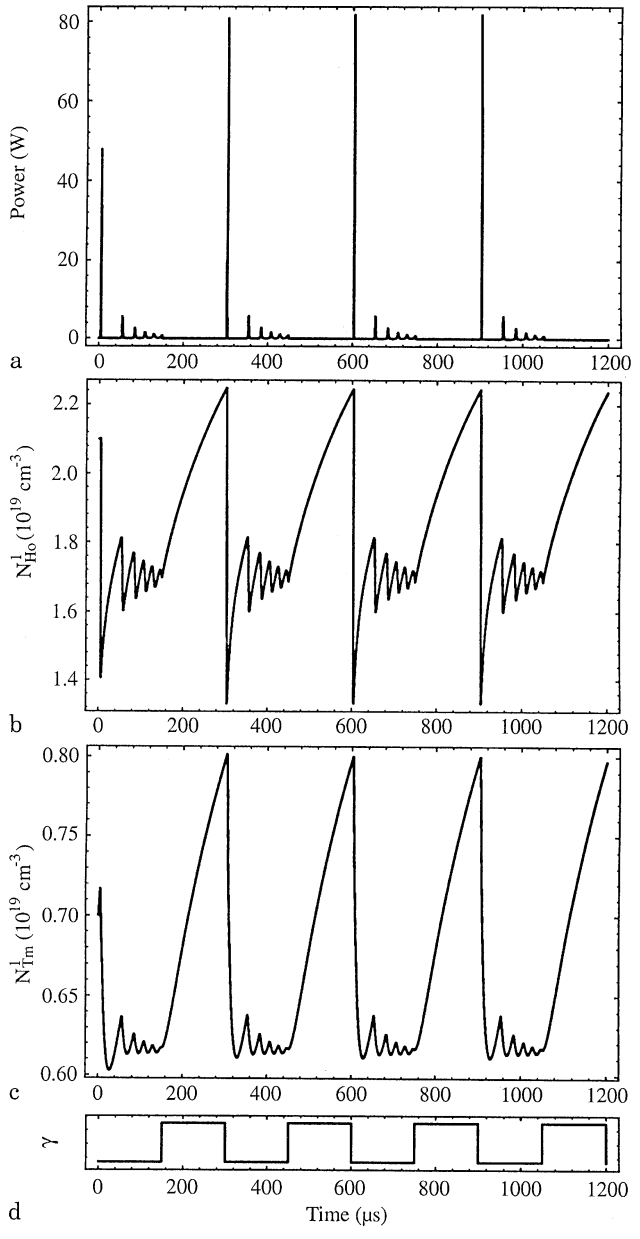

Fig. 8a–d. Higher repetition rate dynamics of Q-switched Tm,Ho:YAG laser (PRF = 3.3 kHz). **a** Laser output. **b** Excited-state Ho population. **c** Excited-state Tm population. **d** Loss modulation function timing

value of $\tau_{Tm\leftrightarrow Ho} = 1$ ns; this situation actually simulates an ultrafast energy transfer. Figure 9a and b shows the results. Figure 9c shows the computed behaviour for the case of laser-normal-mode operation. The first pulse has an energy of 101 μJ and a duration of 0.28 μs, and the second pulse has an energy of 16 μJ and a duration of 1.82 μs. We observe a 46% increase in pulse energy with respect to the previous results $\tau_{Tm\leftrightarrow Ho} = 10$ μs; see Fig. 7). Now, the first spiking pulse appears after a larger time delay of 100 μs (Fig. 9) for $\tau_{Tm\leftrightarrow Ho} = 1$ ns, vs 50 μs (Fig. 7) for $\tau_{Tm\leftrightarrow Ho} = 10$ μs. This is a direct consequence of the much more efficient energy extraction represented by the imagined ultrafast energy transfer, clearly suggesting that the somewhat slow and incomplete energy transfer in Tm,Ho:YAG lasers does not allow complete energy extraction from the coupled excited-state system by the first pulse.

We may also note that for $\tau_{Tm\leftrightarrow Ho} = 10$ μs, a significant damping of the oscillations is predicted by our model and indeed observed in experiments.

As we may see from Fig. 7c and Fig. 9c, the relaxation oscillation frequencies ω_{relax} are different in these two situations; to understand this different behavior, a careful investigation of the dependence of ω_{relax} with pumping rate and wavelength was performed, in the small-signal regime [28]. For quasi-three-level systems,

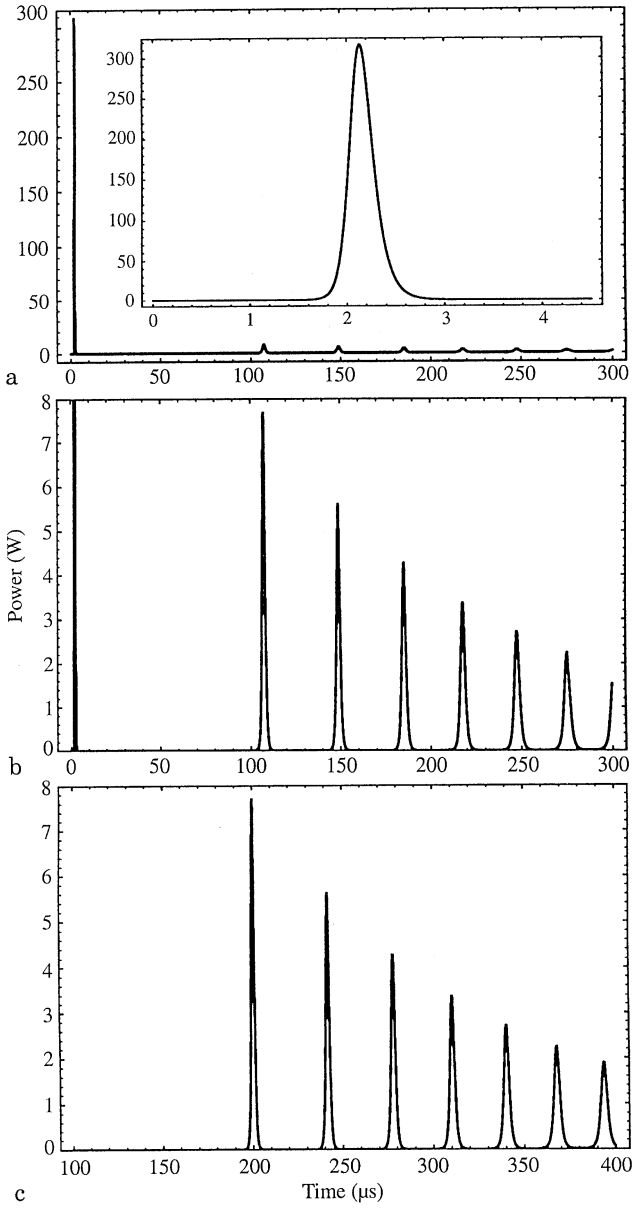

Fig. 9a–c. Computed-output pulses of Tm,Ho:YAG laser (assuming $\tau_{Tm\leftrightarrow Ho} = 1$ ns). **a** Laser in Q-switching regime. Inset shows Q-switched pulse. **b** Expanded vertical scale view. **c** Laser in normal-mode regime. Due to the fast energy transfer time, results b) and c) become indistinguishable

this dependence is

$$\omega_{relax}^2 = (r-1)\gamma\gamma_2\left(1+\frac{\sigma f^0 cNl}{\gamma L}\right). \tag{29}$$

In this expression, $r = P/P_{Th}$ is the pumping rate normalized to the threshold pumping rate, γ is the photon decay rate and γ_2 is the upper-laser-level lifetime. For four-level systems, we have the well-known result

$$\omega_{relax}^2 = (r-1)\gamma\gamma_2. \tag{30}$$

These expressions agree well with simulated and experimental results [28–32], and allow us to distinguish one type of laser system from the other by analyzing the small-signal relaxation oscillations [28].

A significant part of the total available energy for laser action is contained in the spiking pulses that appear after the Q-switched pulse, as previously discussed. For most applications, these pulses are undesirable and parasitic, and a significant effort is usually secured to either eliminate them altogether or at least limit the energy contained in them.

This control is more difficult to achieve in a CW pumped than in a pulsed pumped Q-switched laser. In this later case, we may increase the time delay between the Q-switch opening and the pumping pulse [8]. In a CW pumped laser, we may eliminate these spiking pulses by using a cavity loss modulation function with a small open time [9].

Using an open time of a few tens of μs seems adequate to avoid spiking in single-frequency single-mode lasers. On the other hand, a good energy-extraction efficiency is important, and this leads to an increase in the time delay before the beginning of spiking; thus, high MFs are detrimental to achieve adequate spiking control.

Unfortunately, we have not enough information about the Tm,Ho:YAG upper-level lifetime dependence on the pumping intensity. Nevertheless, we made several model runs for a Q-switched Tm,Ho:YAG laser, allowing the upper-laser-level lifetime value to vary. In all cases, we assumed a low MF (pulse separation much larger than the upper-level lifetime). The results confirm the intuitive feeling that if we assume the pumping power P connected to the upper-laser-level lifetime τ by an expression of the type $P\tau = \text{const}$, then both lasers should generate pulses with approximately the same output energy if we adjust the pumping power accordingly. Up-conversion and other processes are responsible for a strong dependence of the upper-laser-level lifetime on the pumping power. As an example, in some reported experimental conditions [14] the observed effective upper-level lifetime is smaller by a factor of 40 from its value when the pumping intensity is small. We should note that at high pumping rates it may happen that its dependence is stronger than P^{-1} and then we can predict a decrease in Q-switched pulse energy with an increase in pumping rate.

2.3 Conclusions

We developed a detailed rate equation model capable of correctly describing the dynamical behavior of single-and mixed-ion three level solid-state lasers. The model explicitly includes ground-state population depletion, as well as energy distribution among the various fine sublevels in each manifold. We applied this model to the study of continuously pumped and repetitively Q-switched Tm,Ho:YAG and Tm:YAG TEM_{00} single-frequency lasers.

We verified our model by direct comparison with known experimental results [14], and the computational results show very good agreement with the experimental

data. Our model may also be applied to the study of other laser systems based on different laser crystals and operating in normal mode or CW regimes with either CW or pulsed pumping. In addition, our model may also be used for optimizing important laser parameters such as cavity length and mode diameter, cavity design, crystal length, crystal doping levels, Q-switch modulator operation and others.

We also performed an investigation of the spiking process during Q-switched operation of single-frequency Tm,Ho:YAG lasers, and the results showed that the nature of the spiking that appears after the first Q-switched pulse coincides with the spiking occurring in normal-mode laser operation. This suggests that if multiple Q-switched pulses are indeed observed in experiments, then they may be a clear indication of non-single-mode or at least non-single-frequency lasing. A clear conclusion is that for applications requiring true Q-switched pulses, as in laser radars for atmospheric probing, multiple pulse operation should be avoided in principle.

We also found that the optimized laser crystal length for CW operation, regarding lasing threshold, differs from the crystal length that allows maximum power extraction in Q-switching regime; for a pumping power of 4.72 W, and under identical cavity conditions, the optimum crystal length for a Tm:YAG laser was 0.63 cm for CW operation (minimizing lasing threshold) and 2.0 cm for Q-switched operation (maximizing energy extraction). Under Q-switching, a 2.0 cm laser crystal allows the generation of 2.7 mJ pulses at 130 Hz, contrary to just 2.0 mJ pulses predicted for 0.63 cm crystals.

The performance limitations of the Q-switched Tm, Ho:YAG laser compared with the Tm:YAG laser are; the lower upper-level lifetime and the incomplete energy extraction. Using the model we can point that the first is the critical one. In the normal-mode regime these limitations do not contribute significantly to the laser performance, being compensated by the higher Ho laser transition effective cross-section.

The model also indicates that Tm:YAG lasers are more effective for pulse generation than Tm,Ho:YAG lasers, allowing pulses with an order of magnitude higher energy than those obtainable from a Tm,Ho:YAG laser. The model shows that the main reason for the pulse energy decrease on Tm,Ho:YAG is the strong pump power dependence of the upper-level lifetime and not the slow and incomplete energy transfer. When this dependence becomes strong enough, it becomes possible to increase the output-pulse energy by decreasing the pumping power. Reducing the energy transfer time from the normal value of 10 μs to an ultrafast value of 1 ns resulted only in a 50% increase in predicted output energy (85 μJ for 10 μs and 127 μJ for 1 ns, at a PRF of 1 kHz). This does not necessarily exclude mixed crystals like Tm,Ho for high-power pulse generation. Suitable host material like YLF and LuAG [33], with adequate upper-level lifetime and no strong up-conversion effects present may be suitable candidates for efficient pulsed operation.

In conclusion, our model gives reliable results for output pulse energy, pulse temporal shape, and level population dynamics for both Tm,Ho:YAG and Tm:YAG laser systems, when we compare our results with previously published experimental measurements. We attribute the dicrepancy in pulse duration to the fact that our model does not yet include a full spatial (3D) analysis in the rate equations.

Acknowledgements. The research presented in this paper was performed as part of the European Project BRITE-EURAM FLAME (Future Laser Atmospheric Measurement Equipment), CEC Contract AERO-CT92-0045.

References

1. T.Y. Fan, D.F. Welch: IEEE J. Quantum Electron. **QE-28**, 940–941 (1992)
2. H. Combe: "*FLAME system analysis*, *Final Report Task* 1.1: *system requirements*", Internal Project Report, September (1993)
3. T.Y. Fan, G. Huber, R.L. Byer, P. Mitzscherlich: IEEE J. Quantum Electron. **QE-24**, 924–933 (1988)
4. G.M. Zverev, G.Ya. Kolodnyi, A.M. Onishchenko: Sov. Phys. JETP **30**, 435–440 (1970)
5. N.P. Barnes and D.J. Gettemy: Appl. Opt. **29**, 404–409 (1990)
6. R.C. Stoneman and L. Esterowitz: Opt. Lett. **17**, 736–738 (1992)
7. M.E. Storm: Appl. Opt. **27**, 4170–4172 (1988)
8. K.K. Kim, Y.S. Choi, N.P. Barnes, R.V. Hess, C.H. Bair, P. Brockman: Appl. Opt. **32**, 2066–2074 (1993)
9. S.R. Bowman, M.J. Winings, S. Searles and B.J. Feldman: IEEE J. Quantum Electron. **27**, 1129–1131 (1991)
10. J.B. Gruber, M.E. Hills, R.R Macfarlane, C.A. Morrison, G.A. Turner, G.J. Quarles, G.J. Kintz, L. Esterowitz: Phys. Rev. B **40**, 9464–9478 (1989)
11. E.D. Filer, N.P. Barnes, C.A. Morrison: In *OSA Proc. on Advanced Solid State Lasers*, Vol. 10, (1991) pp. 189–200
12. A.A. Kaminskii: *Laser Crystals* (Springer-Verlag, Berlin, 1990) Chap. 5
13. G.M. Zverev, G.Ya. Kolodnyi, A.M. Onishchenko: Sov. Phys. JETP **30**, 435–440 (1971)
14. T.S. Kubo and T.J. Kane: IEEE J. Quantum Electron. **QE-28**, 1033–1040 (1992)
15. E.P. Chicklis, R.C. Folweiler, C.S. Naiman, D.R. Gabbe, A. Linz, H.P. Jennssen: Tech. Rep. ECOM-73-0066-F, Oct. 1974
16. G.J. Kuntz, R. Allen, L. Esterowitz: In *Postdeadline Papers*, *Conf. on Lasers and Electro-Opt*., Opt. Soc. Amer., Washington DC, 1987, Paper ThU4
17. J.B. Gruber, M.E. Hills, M.D. Seltzer, S.B. Stevens, C.A. Morrison, G.A. Turner, M.R. Kokta: J. Appl. Phys. **69**, 8183–8204 (1991)
18. M.Kh. Ashurov, Yu.K. Voronko, E.V. Zharikov, A.A. Kaminskii, V.V. Osiko, A.A. Sobol, M.I. Timoshechkin, V.A. Fedorov, A.A. Shabaltai: Inorg. Mater. **15**, 979–983 (1979)
19. E.D. Filer, C.A. Morrison, G.A. Turner, N.P. Barnes: In *Advanced Solid State Lasers*, Vol. 6, *OSA Proc. Series*, Washington (1990) pp. 354–370
20. S.W. Henderson, C.P. Hale, and J.R. Magee: In *Advanced Solid State Lasers*, Vol. 6, *OSA Proc.* Series, Washington (1990) pp. 127–133
21. D.E. Castleberry: Ph.D. Dissertation, Massachusetts Inst. Technol., Cambridge (1975)
22. B.M. Antipenko, A.S. Glebov, T.I. Kiseleva, V.A. Pismennyi Opt. Spectrosc. **60**, 95–97 (1986)
23. P.J.M. Suni and S.W. Henderson: Opt. Lett. **16**, 817–819 (1991).
24. T.Y. Fan, R.L. Byer: IEEE J. Quantum Electron. **QE-23**, 605–612 (1987)
25. S.R. Bowman, G.J. Quarlews, B.J. Feldmad: In *OSA Proc. on Advanced Solid State Lasers*, Vol. 13, (1992) pp. 169–173
26. A. Cassanho, H.P. Jenssen, M.A. Noginov, V.G. Ostroumov, G.Q. Sarkissian, I.A. Shcherbacov, V.A. Smirnov: In *OSA Proc. on Advanced Solid State Lasers*, Vol. 13, (1992) pp. 300–305

27. L.L. Chase, S.A. Payne, L.K. Smith, W.L. Kway, W.F. Krupke: In *OSA Proc. on Advanced Solid State Lasers*, Vol. 10 (1991) pp. 161–165
28. J.R. Salcedo, J.M. Sousa, V.V. Kuzmin: Appl. Phys. B **62**, 83–85 (1996)
29. O.G. Okhotnikov, V.V. Kuzmin, J.R. Salcedo: IEEE Photonics Lett. **6**, 362–364 (1994)
30. O.G. Okhotnikov, J.R. Salcedo: Opt. Lett. **19**, 1445–1447 (1994)
31. O.G. Okhotnikov, J.R. Salcedo: *EQEC*' 94, paper QTuB6, Amsterdam (1994) p. 40
32. O.G. Okhotnikov, J.R. Salcedo: IEEE Photonics Lett. **6**, 369–371 (1994)
33. J.R. Hobbs: *Diodes pump Ho,Tm:LuAG Crystal Efficiently*, Laser Focus World, May, (1994) pp. 55–56